Wide-Swath Ocean Topography using Formation Flying Under Squinted Geometries
The Harmony Mission Case

Theodosiou, Andreas; Kleinherenbrink, Marcel ; Lopez Dekker, Paco

DOI
10.1109/IGARSS47720.2021.9554076

Publication date
2021

Document Version
Final published version

Published in
2021 IEEE International Geoscience and Remote Sensing Symposium IGARSS

WIDE-SWATH OCEAN TOPOGRAPHY USING FORMATION FLYING UNDER SQUINTED GEOMETRIES: THE HARMONY MISSION CASE

Andreas Theodosiou, Marcel Kleinherenbrink, Paco López-Dekker

Delft University of Technology
Geoscience and Remote Sensing
The Netherlands

ABSTRACT

Ocean topography using SAR interferometry requires coherent observations of the sea surface. To observe the surface coherently, the along-track baseline between observations of the same scene must be kept to a minimum. Minimising the along-track baseline while maintaining a cross-track baseline that allows good sensitivity to relative surface height is difficult to achieve in satellite missions. This paper shows how a squinted line of sight allows single-pass cross-track interferometry with a wide swath over oceans. The Harmony candidate mission will have a formation that uses such an acquisition geometry to coherently observe the oceans.

Index Terms— SAR, InSAR, bistatic SAR, sea surface height, squinted line of sight, ocean topography

1. INTRODUCTION

The ocean is a key component of the climate system, receiving the majority of solar radiation that reaches the Earth's surface as heat. Changes in ocean heat content are largely driven by climate and result in ocean level variability. Our understanding of ocean circulation and sea level change is therefore important both to oceanography and to climate science. Satellites, mainly altimeters, have contributed to our understanding by providing a measure of the sea surface height (SSH).

Cross-track interferometry (XTI) provides measures of height using the phase differences of echoes from an imaged region received at two antennas that are displaced from one another [1]. Missions such as TanDEM-X have demonstrated that interferometric SAR can produce accurate digital elevation models (DEM) of land masses. Topographic mapping of the ocean surface remains a challenge due to the quick temporal decorrelation of the surface.

Single-pass XTI uses large cross-track baselines to increase the sensitivity to the surface elevation. Along-track baselines result in a time lag between the images of the same region from the two SARs, which lead to decorrelation between the two images. Over land, moderate temporal decorrelation is often not a problem due to the fact that the ground is not rapidly changing during the time between the two acquisitions. Over the oceans, however, the rapidly changing sea surface sets strict requirements on the along-track baseline.

SAR satellites can be flown in a formation to achieve more performant interferometric baselines between the sensors. The Helix formation [2] allows cross-track baselines while limiting the along-track baselines. In a Helix formation, the radial (vertical) separation results in an along-track baseline that tends to a minimum at polar latitudes and a maximum at mid-latitudes.

In zero-Doppler SAR interferometry, where line-of-sight (LoS) is perpendicular to the flight direction, maximum along-track baseline at mid-latitudes does not facilitate topographic mapping of the oceans. In this paper we propose using a squinted LoS to decrease the effective along-track baseline of an interferometer and allow coherent measurements of relative sea-surface heights (SSH).

Harmony [3], a candidate mission for Earth Explorer 10, with its squinted LoS and bistatic formation will provide a suitable system to topographically map the ocean surface over wide swaths. In the following sections we will present the performance analysis of relative SSH obtained by SAR interferometry with a squinted LoS, taking Harmony as the example.

2. METHODOLOGY

An overview of the process used to arrive to the estimate of the error in the SSH measurement is illustrated in Figure 1. The elevation estimate and its uncertainty depend on the acquisition geometry, the sensitivity of the instrument, the surface, the coherence and the number of independent looks.

2.1. Acquisition Geometry

2.1.1. Formation Flying

The orbital frame of reference is used as the basis for all the calculations. It consists of three unit vectors moving together: $\hat{e}_R$ along the radial direction (positive away from the Earth's centre), $\hat{e}_T$ in the along-track (tangential) direction

IGARSS 2021 - 2021 IEEE International Geoscience and Remote Sensing Symposium | 978-1-6654-0369-6/21/$31.00 ©2021 IEEE | DOI: 10.1109/IGARSS47720.2021.9554076

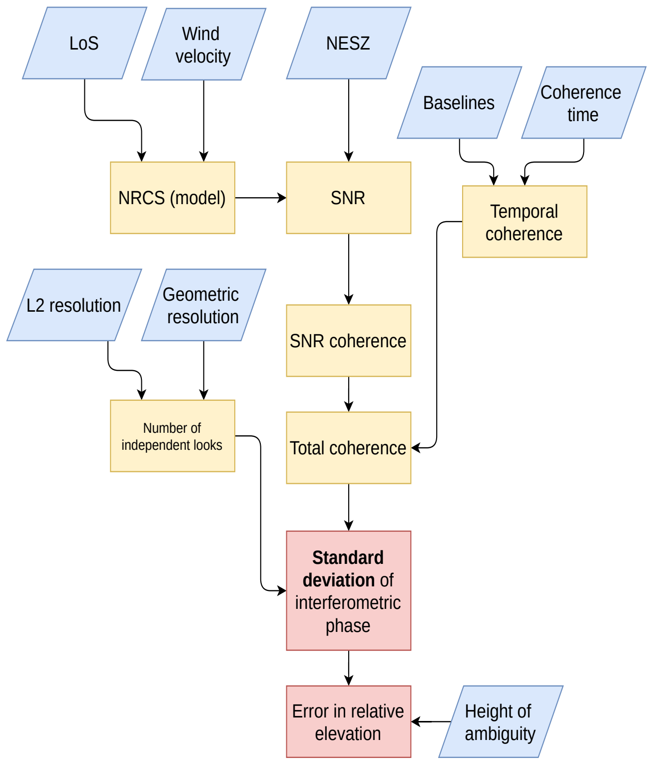

Fig. 1: Process of computing the SSH error.

of the satellite motion, and the unit vector $\hat{e}_N$ normal to the orbital plane in direction of the positive angular momentum vector (cross track).

For near-circular orbits in close formation, which is the case for Harmony, the relative motion $\Delta\vec{r}$ can be expressed linearly [2]

$$\begin{aligned}\Delta r_T &= -2\alpha\Delta e\cos(u-\phi)+\Delta x_T,\\ \Delta r_N &= -a\Delta i\cos(u),\\ \Delta r_R &= -a\Delta e\sin(u+\phi),\end{aligned} \tag{1}$$

where a is the semi-major axis of the orbit, Δe and Δi are the norms of the difference between the eccentricity and inclination vectors respectively, u is the mean argument of latitude and ϕ is the relative perigee.

2.1.2. Along-track Baseline

In a zero Doppler configuration, squint angle $\theta_s = 0$, the along-track baseline relevant to interferometry is equal to the physical separation of the two satellites in the tangential direction. In cases where $-\frac{\pi}{2} < \theta_s < \frac{\pi}{2}$, the baseline that arises due to the temporal lag between two observations is no longer the same as the physical separation.

The squinted LoS and the cross-track separation cause the second satellite to observe the same point on the ground after it has moved

$$B_{\mathrm{ATI}} = \Delta r_T - \Delta r_N \tan\theta_s, \tag{2}$$

in the along-track direction.

2.1.3. Cross-track Baseline

The baseline, $B_\perp$, is the distance between the two satellites in the perpendicular direction to the LoS. In the case of zero squint, the cross-track baseline is determined by the incident angle, θ_i, Δr_N, and Δr_R.

Introducing a squint to the LoS changes the effective baseline, as was the case for along track interferometry. The effective baseline depends on the LoS and the co-registration. The unit vector pointing in the direction of the LoS is represented by $\hat{e}_{\mathrm{LoS}}$. At the point where the two satellites view the same point on the ground, their separation is given by

$$\vec{b} = \begin{pmatrix}\Delta r_R\\ \Delta r_N\tan\gamma\\ \Delta r_N\end{pmatrix}, \tag{3}$$

where $\tan\gamma$ is the ratio of the along-track component to the normal component of $\hat{e}_{\mathrm{LoS}}$. The effective baseline is given by

$$B_\perp = \left\|\vec{b}\right\|\sin\psi = \left\|\vec{b}\times\hat{e}_{\mathrm{LoS}}\right\|, \tag{4}$$

where ψ is the angle between $\vec{b}$ and the LoS unit vector.

2.1.4. Harmony

Harmony consists of two passive companion satellites, Concordia and Discordia, flying in formation with Sentinel-1 as the illuminator. In the XTI mission phase, Concordia and Discordia will fly in a double-Helix formation with a cross-track separation of several hundred meters, as show in Figure 2.

For the purposes of the analysis in the following sections, the interferometric baselines between the companion satellites are computed by assuming that Concordia and Discordia are monostatic SARs with an equivalent line of sight that equals the mean line of sight of the illuminator and the companion.

2.2. Interferometric Model

The interferometric phase measured by Harmony, $\Delta\phi$, will have contributions both from the topography of the scene, ϕ_{topo}, and from movement in the direction of the line of sight ϕ_{ATI}, due to the cross-track baseline and along-track baseline respectively. The measurement will also include a random noise term, ϕ_n

$$\Delta\phi = \phi_{\mathrm{topo}} + \phi_{\mathrm{ATI}} + \phi_n, \tag{5}$$

The phase due to the along-track baseline, ϕ_{ATI}, is estimated by the two-channel receiver system on-board each of

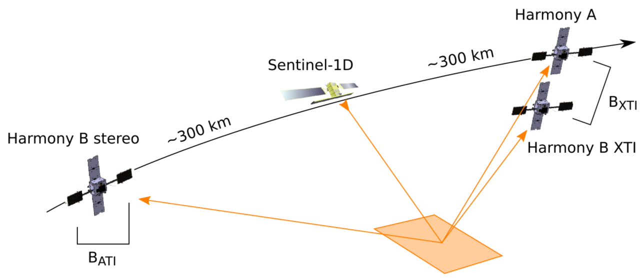

Fig. 2: The two Harmony configurations. In the XTI configuration the two companions fly in close formation. In the stereo configuration one companion leads Sentinel-1 and the other trails it. Figure taken from [4].

the Harmony satellites. The two channels have a physical separation along the track, making them sensitive to movement in the direction parallel to the line of sight. The estimate of this phase, $\hat{\phi}_{\mathrm{ATI}}$, is subtracted from the measured phase to remove the undesired ATI component, giving an estimate of the phase due to the topography of the scene $\hat{\phi}_{\mathrm{topo}}$.

The estimation error, ϵ_{ATI}, adds to the total error of the measurement, such that

$$\hat{\phi}_{\mathrm{topo}} = \phi_{\mathrm{topo}} + \epsilon_{\mathrm{ATI}} + \phi_n, \tag{6}$$

$$\epsilon_{\mathrm{ATI}} = \phi_{\mathrm{ATI}} - \frac{B_{\|}}{B_{\|s}} \hat{\phi}_{\mathrm{ATI}}, \tag{7}$$

where the estimate of along-track phase contribution acquired using the short baseline is scaled by the ratio of the formation along-track baseline to the along-track baseline of the onboard phase centres. The scaling factor arises due to the linearly proportional relationship between the phase and the along-track baseline. Thus, the smaller baseline between the on-board passive channels produces a smaller phase for a given Doppler shift.

The standard deviation of the relative surface height is used as a measure of SSH uncertainty. The interferometric phase, $\Delta\phi$ and relative surface height, Δh are related by

$$\Delta h = \frac{h_{\mathrm{amb}}}{2\pi} \Delta\phi, \tag{8}$$

where h_{amb} is the height of ambiguity. We use the Cramer-Rao lower bound [5] for the phase standard deviation

$$\sigma_\phi = \sqrt{\frac{1-\gamma^2}{2N_l\gamma^2}}, \tag{9}$$

where γ is the coherence and N_l is the number of independent looks.

2.3. Coherence Estimation

The coherence is the product of

$$\gamma \approx \gamma_{\mathrm{SNR}} \gamma_t \gamma_{\mathrm{Quant}} \gamma_{\mathrm{Amb}} \gamma_{\mathrm{Vol}}, \tag{10}$$

where the right-hand side of the equation describes the contributions to the error due to noise (γ_{SNR}), temporal decorrelation (γ_t), quantisation (γ_{Quant}), ambiguities (γ_{Quant}), and volume decorrelation (γ_{Vol}).

The coherence due to noise depends on the SNR , which is a function of the NESZ and the backscatter coefficient of the mapped pixel

$$\gamma_{\mathrm{SNR}} = \frac{1}{1 + \mathrm{SNR}\left(\sigma^0, \mathrm{NESZ}\right)^{-1}}. \tag{11}$$

In the following analysis the NESZ of Harmony is computed over the IW swath of S-1 and the backscatter is modelled using the bistatic model presented in [6] with a wind of $5\,\mathrm{m\,s^{-1}}$ in the downwind direction.

The coherence due to temporal decorrelation consists of one component due to the cross-track baseline [7] and another one due to the time-lag in the along-track direction [8]

$$\gamma_t = \gamma_{\mathrm{XTI}} \gamma_{\mathrm{ATI}}, \tag{12}$$

$$\gamma_{\mathrm{XTI}} = 1 - \frac{B_\perp}{B_{\perp,c}}, \tag{13}$$

$$\gamma_{\mathrm{ATI}} = \mathrm{e}^{-\tau^2/\tau_c^2}, \tag{14}$$

where $B_{\perp,c} = \frac{\lambda r}{m \rho_y \cos^2(\theta-\alpha)}$ is the crictical across-track baseline at range resolution ρ_y, $\tau = \frac{B_{\|}}{2v}$ is the time lag between acquisitions due to the effective along-track baseline $\frac{B_{\|}}{2}$ and platform velocity v, and $\tau_c \approx 3.29\lambda/U$ is the coherence time at wind speed U.

The number of independent looks is the ratio of the product resolution and nominal geometric resolution. For Sentinel-1 in IWS mode the spatial resolution is $5 \times 20\ \mathrm{m}^2$; Setting the level-2 resolution of the product Harmony will produce is dependent on the accuracy we want to achieve. For relative elevation measurements with accuracy of $10\ \mathrm{cm}$, $8 \times 8\ \mathrm{km}^2$ is sufficient, corresponding to 64×10^3 samples.

Using the coherence factors, the interferometric phase noise, ϕ_n and the estimation error, ϵ_{ATI} are computed. The height uncertainty is computed by substituting ϕ_n and ϵ_{ATI} into (8).

3. RESULTS

The estimated sea surface error for a given set a of formation parameters is shown in Figure 3. The error is in the order of $10\,\mathrm{cm}$ over the majority of the swath, throughout the orbit, with the exception of the poles over the swath of Sentinel-1. The best performance is achieved near the Equator because at that point the formation has the largest cross-track baseline.

The performance shown in Figure 3b has the potential to allow for coherent observations of the ocean surface at submesoscales. The two different formations show that the formation parameters can be used to optimise the performance at different points along the swath.

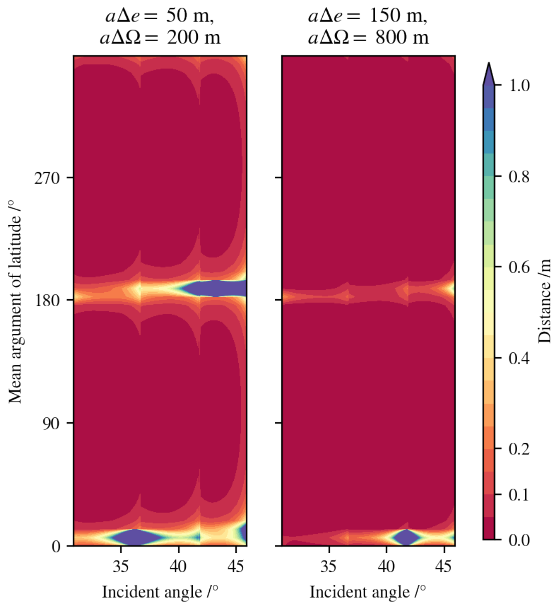

(a) Uncertainty due to noise.

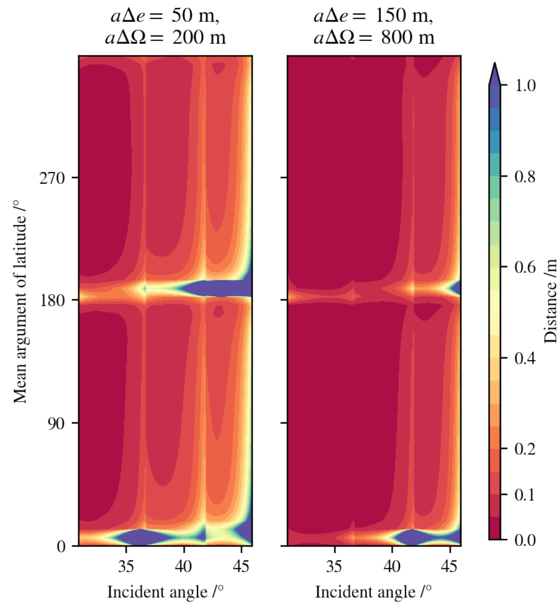

(b) Total uncertainty.

Fig. 3: The estimated SSH uncertainty in terms of 1σ. $\Delta\Omega$ is the difference in the right ascension of the ascending node between the two companions.

4. CONCLUSIONS

One of the challenges of SAR interferometry over the oceans is the trade-off between coherent observation of the ocean surface and large baselines to provide high sensitivity to height. A SAR interferometer with a squinted LoS flying in a formation with parameters chosen for XTI could minimise along-track baselines while maintaining large cross-track baselines. In other words, coherent observations of the surface with high sensitivity to height.

The benefits of this approach are: the capability to fully capture mesoscale feature on a high-resolution grid; cross-track sampling with respect to altimeters; capability to estimate cross-track SSH slopes. Harmony will be the first satellite mission that will offer the opportunity to test this concept.

5. REFERENCES

[1] Howard A. Zebker and Richard M. Goldstein, "Topographic mapping from interferometric synthetic aperture radar observations," vol. 91, pp. 4993–4999.

[2] Simone D'Amico and Oliver Montenbruck, "Proximity operations of formation-flying spacecraft using an eccentricity/inclination vector separation," *Journal of Guidance, Control, and Dynamics*, vol. 29, no. 3, pp. 554–563, 2006.

[3] P. López-Dekker, H. Rott, P. Prats-Iraola, B. Chapron, K. Scipal, and E. D. Witte, "Harmony: an earth explorer 10 mission candidate to observe land, ice, and ocean surface dynamics," in *IGARSS 2019 - 2019 IEEE International Geoscience and Remote Sensing Symposium*, 2019, pp. 8381–8384.

[4] M. Kleinherenbrink, A. Korosov, T. Newman, A. Theodosiou, Y. Li, G. Mulder, P. Rampal, J. Stroeve, and P. Lopez-Dekker, "Estimating instantaneous sea-ice dynamics from space using the bi-static radar measurements of earth explorer 10 candidate harmony," *The Cryosphere Discussions*, vol. 2020, pp. 1–25, 2020.

[5] M.S. Seymour and I.G. Cumming, "Maximum likelihood estimation for SAR interferometry," in *Proceedings of IGARSS '94 - 1994 IEEE International Geoscience and Remote Sensing Symposium*, vol. 4, pp. 2272–2275 vol.4.

[6] Yan Yuan, "Modulation of radar observables by upper ocean dynamics," 2020.

[7] Howard A Zebker, John Villasenor, et al., "Decorrelation in interferometric radar echoes," *IEEE Transactions on geoscience and remote sensing*, vol. 30, no. 5, pp. 950–959, 1992.

[8] S. J. Frasier and A. J. Camps, "Dual-beam interferometry for ocean surface current vector mapping," *IEEE Transactions on Geoscience and Remote Sensing*, vol. 39, no. 2, pp. 401–414, 2001.